https://doi.org/10.1093/plphys/kiac221 PLANT PHYSIOLOGY 2022: 189: 2175–2192

Plant Physiology®

Research Article

An Arabidopsis *pre-RNA processing8a (prp8a)* missense allele restores splicing of a subset of mis-spliced mRNAs

Roxanna J. Llinas [1], **Jia Qi Xiong** [1,†], **Natalie M. Clark** [2], **Sarah E. Burkhart** [1] and **Bonnie Bartel** [1,*,‡]

1 Department of Biosciences, Rice University, Houston, Texas 77005, USA
2 Department of Plant Pathology and Microbiology, Iowa State University, Ames, Iowa 50011, USA

*Author for correspondence: bartel@rice.edu
†Present address: Baylor College of Medicine, Houston, Texas 77030, USA
‡Senior author

R.J.L. conducted most of the experiments, analyzed the data, prepared the figures, and wrote the manuscript with input from all authors. J.Q.X. assisted with some of the experiments. N.M.C. conducted the bioinformatic analysis and assisted with bioinformatic data interpretation. S.E.B. conducted the original *pex14-6* suppressor screen. B.B. conceived the original screen, supervised the experiments, and assisted with data analysis. B.B. agrees to serve as the author responsible for contact and ensures communication.
The author responsible for distribution of materials integral to the findings presented in this article in accordance with the policy described in the Instructions for Authors (https://academic.oup.com/plphys/pages/general-instructions) is Bonnie Bartel (bartel@rice.edu).

Abstract

Eukaryotic precursor mRNAs often harbor noncoding introns that must be removed prior to translation. Accurate splicing of precursor messenger RNA depends on placement and assembly of small nuclear ribonucleoprotein (snRNP) sub-complexes of the spliceosome. Yeast (*Saccharomyces cerevisiae*) studies established a role in splice-site selection for PRE-RNA PROCESSING8 (PRP8), a conserved spliceosome scaffolding protein of the U5 snRNP. However, analogous splice-site selection studies in multicellular eukaryotes are lacking. Such studies are crucial for a comprehensive understanding of alternative splicing, which is extensive in plants and animals but limited in yeast. In this work, we describe an Arabidopsis (*Arabidopsis thaliana*) *prp8a* mutant that modulates splice-site selection. We isolated *prp8a-14* from a screen for suppressors of *pex14-6*, which carries a splice-site mutation in the *PEROXIN14* (*PEX14*) peroxisome biogenesis gene. To elucidate Arabidopsis PRP8A function in spliceosome fidelity, we combined *prp8a-14* with various *pex14* splice-site mutations and monitored the double mutants for physiological and molecular consequences of dysfunctional and functional peroxisomes that correspond to impaired and recovered splicing, respectively. *prp8a-14* restored splicing and PEX14 function to alleles with mutations in the exonic guanine of the 5′-splice site but did not restore splicing or function to alleles with mutations in the intronic guanine of 5′- or 3′-splice sites. We used RNA-seq to reveal the systemic impact of *prp8a-14* and found hundreds of differentially spliced transcripts and thousands of transcripts with significantly altered levels. Among differentially spliced transcripts, *prp8a-14* significantly altered 5′- and 3′-splice-site utilization to favor sites resulting in shorter introns. This study provides a genetic platform for probing splicing in plants and hints at a role for plant PRP8 in splice-site selection.

Introduction

Splicing is an essential step in eukaryotic protein production that processes precursor messenger RNAs (pre-mRNAs) to remove introns, which interrupt coding regions of the pre-mRNA. Various mRNA products can arise from one gene through differential exon ligation in a phenomenon termed

Received November 19, 2021. Accepted April 19, 2022. Advance access publication May 24, 2022

alternative splicing. Alternative splicing expands proteome diversity without concurrent genome expansion. This compressed storage of genetic information partially explains why genome size does not track linearly with organism complexity (Nilsen and Graveley, 2010; Chen et al., 2014).

Alternative splicing is relatively common and can augment protein diversity. However, examples of actual contributions to protein diversity are sparse, and proteomic support for much of the observed mRNA diversity is lacking (Chaudhary et al., 2019). Examples of effectual alternative splicing in human biology include the regulation of immunoglobulin production in B cells (Early et al., 1980; reviewed in Schaub and Glasmacher, 2017) and T-cell differentiation through differential splicing of *PTPRC*, which encodes Protein Tyrosine Phosphatase Receptor Type C to make various protein isoforms (reviewed in Schaub and Glasmacher, 2017). In addition, cardiac muscle development relies on alternative splicing of *TITIN* to produce flexible muscles in infant hearts and rigid muscles in adult hearts (Linke, 2008). In plants, examples of regulation via intron retention and subsequent nonsense-mediated mRNA decay include *LATE ELONGATED HYPOCOTYL* (*LHY*), *PSEUDO RESPONSE REGULATOR7* (*PRR7*), and *CIRCADIAN CLOCK ASSOCIATED1* (*CCA1*), which control the circadian clock (reviewed in Chaudhary et al., 2019). As in humans, there are only a few documented cases of functional protein isoforms derived from alternatively spliced plant mRNAs. One example is the cold-induced alternative splicing of the Arabidopsis (*Arabidopsis thaliana*) transcription factor gene *INDERMINATE DOMAIN14* (*IDD14*), which results in a nonfunctional protein that binds to and inhibits the functional isoform (Seo et al., 2011).

Intron removal and exon ligation are performed by the spliceosome (Brody and Abelson, 1985), a dynamic molecular machine composed of five main RNA–protein subcomplexes (reviewed in Lerner et al., 1980; Galej, 2018). These sub-complexes are small nuclear ribonucleoproteins (snRNPs) named U1, U2, U4, U5, and U6 (Lerner and Steitz, 1979; Black et al., 1985; Chabot et al., 1985; Krainer and Maniatis, 1985; Black and Steitz, 1986; Winkelmann et al., 1989) after the small nuclear RNA (snRNA) that they contain (Lerner and Steitz, 1979). snRNPs bind to a pre-mRNA at splice sites flanking an intron and specify which pre-mRNA region is removed (Zhuang and Weiner, 1986; Seraphin et al., 1988; Siliciano and Guthrie, 1988). The snRNPs assemble in a highly orchestrated manner and recruit other protein complexes to facilitate the multiple steps of pre-mRNA processing (Mount et al., 1983; Konarska and Sharp, 1987; Seraphin and Rosbash, 1989; Seraphin et al., 1991). To complete the two transesterification reactions that remove an intron and ligate adjacent exons (Konarska et al., 1985), the spliceosome cycles through ten conformations with varying compositions of snRNPs and facilitating proteins (Fabrizio et al., 2009; reviewed in Hoskins et al., 2011; Galej, 2018).

Consensus sequences define the splice sites at the 5′ and 3′ ends of an intron (Rogers and Wall, 1980; Mount, 1982) and at a catalytically important intronic adenine upstream of the 3′-splice site that is the lariat branch point (Domdey et al., 1984; reviewed in Galej, 2018). The *U1* and *U2* snRNAs (in the corresponding snRNPs) base pair with the 5′-splice site and branch site to precisely position spliceosome assembly on the pre-mRNA and ensure 5′-splice-site recognition (Zhuang and Weiner, 1986; Parker et al., 1987). The U4, U5, and U6 snRNPs then bind to the U1 and U2 snRNPs (Cheng and Abelson, 1987; Konarska and Sharp, 1987; reviewed in Wahl et al., 2009). After snRNP assembly, additional facilitating proteins associate and release to rearrange the spliceosome–pre-mRNA assembly into the catalytically active conformation (reviewed in Galej, 2018).

The core U5 snRNP remains present as hundreds of proteins transiently associate with the spliceosome during an assembly and catalysis cycle. The largest protein of the U5 subcomplex is PRE-RNA PROCESSING8 (PRP8), a highly conserved structural protein that coordinates placement of other snRNPs and the pre-mRNA (Galej et al., 2013). PRP8 interacts with the 5′- and 3′-splice sites and the branch site to position the 5′- and 3′-exons in the spliceosome active site (Turner et al., 2006). Between the first and second catalytic steps, the PRP8 RNaseH-like domain moves to reorient the pre-mRNA and juxtapose the 5′- and 3′-splice sites. The position of the RNaseH-like domain promotes either the first or second catalytic step (reviewed in Liu et al., 2007; Galej et al., 2013).

Two genes encode PRP8 in Arabidopsis: *PRP8A* (*At1g80070*) and *PRP8B* (*At4g38780*). *PRP8A* is more highly expressed than *PRP8B*, and *prp8a* null mutations are lethal (Schwartz et al., 1994; Marquardt et al., 2014). In contrast, insertional alleles of the less-expressed *PRP8B* are viable but display female gametophytic defects in combination with *prp8a* mutants (Kulichová et al., 2020). Several viable *prp8a* missense alleles displaying reduced splicing efficiency have been characterized, including *prp8a-6*, *prp8a-7*, *prp8a-10*, and *prp8a-11* (Marquardt et al., 2014; Sasaki et al., 2015; Kanno et al., 2017).

In addition to loss-of-function alleles, gain-of-function *prp8* alleles have been identified in Arabidopsis and in the yeast *Saccharomyces cerevisiae*. These gain-of-function *prp8* mutations were isolated using suppression screens for secondary mutations that improved splicing in an original mutant with defective splicing. For example, spliceosome assembly is impaired in an Arabidopsis *protein arginine methyltransferase5* (*prmt5*) mutant, and the *prp8a-8* and *prp8a-9* missense alleles restore splicing in *prmt5* by improving prp8a association with a stabilizing protein complex, thus restoring spliceosome assembly and function (Deng et al., 2016). In yeast, pre-mRNAs with mutated splice-site consensus sequences that disrupt recognition by the spliceosome were used to screen for *prp8* mutants that restore splicing (Collins and Guthrie, 1999; Query and Konarska, 2004). These *prp8* mutants illuminated splice-site fidelity,

spliceosome recognition, and the role of PRP8 in splice-site selection.

In an investigation of peroxisome function in plants, we employed a suppression screen approach. We screened for suppressors of *pex14-6*, a mutant with an altered 5′-splice site that disrupts *PEX14* RNA processing, reduces PEX14 protein accumulation, and impairs peroxisome function (Burkhart et al., 2013). Screening the progeny of mutagenized *pex14-6* plants for suppressors with improved peroxisome function yielded a suppressor that restored protein levels and mRNA splicing to *pex14-6*, and we identified a causal mutation in *PRP8A*. This mutant represents an Arabidopsis splicing factor allele that recognizes noncanonical splice-site sequences.

Results

Identification of a *prp8a* missense allele as a *pex14-6* suppressor with improved IBA responsiveness

We isolated a *prp8a* mutant as a suppressor of *pex14-6*, a mutant arising from mis-splicing of the *PEX14* gene (Burkhart et al., 2013). PEX14 is a crucial peroxisome biogenesis protein (Azevedo and Schliebs, 2006). Consequently, *pex14-6* peroxisomes inefficiently import enzymes into the lumen of peroxisomes, which slows the processing of indole-3-butyric acid (IBA) into the active phytohormone auxin, indole-3-acetic acid (IAA; Burkhart et al., 2013). In wild-type seedlings grown on IBA-supplemented media, IAA derived from peroxisomally metabolized IBA limits root cell elongation, slowing root growth (Figure 1A; Zolman et al., 2000). In contrast, *pex14-6* peroxisomes inefficiently convert IBA into IAA, allowing roots to elongate despite the presence of IBA (Figure 1A; Burkhart et al., 2013). We identified suppressors by growing the progeny of ethyl methanesulfonate (EMS)-mutagenized *pex14-6* on IBA and screening for individuals with short roots indicative of restored peroxisome function (Figure 1A).

We used whole-genome sequencing of backcrossed lines to identify mutations in one *pex14-6* suppressor (Figure 1B). Because *pex14-6* is a mis-splicing allele, which might be repaired by modifying the splicing machinery, we searched the genes carrying nonsynonymous mutations for those related to splicing and found a missense mutation in *PRP8A*/*At1g80070* (Figure 1D). PRP8 is a critical component of the U5 snRNP that coordinates pre-mRNA positioning within the spliceosome. The identified mutation in exon 13 would change the conserved Gly1326 to Arg (Figure 1, D and F) in the Thumb/X domain (Figure 1E), which interacts with the *U5* snRNA as well as the 5′ and branch point splice sites (Turner et al., 2006).

We determined that the identified *prp8a* mutation was linked to the causal suppressing mutation by examining IBA responsiveness of the progeny of the suppressor backcrossed to *pex14-6*. Seedlings that were homozygous for *pex14-6* and segregating for the suppressing mutation were scored for IBA root sensitivity and then individually genotyped for the *prp8a* mutation. We found that *prp8a pex14-6* seedlings displayed wild-type IBA responsiveness and *PRP8A pex14-6* seedlings were IBA resistant (Figure 1C), confirming linkage of the causal mutation to the *prp8a* locus. Like the homozygous double mutant, *PRP8A*/*prp8a pex14-6*/*pex14-6* seedlings displayed improved IBA responsiveness (Figure 1C). This semi-dominance suggests that the *prp8a* Gly1326-to-Arg mutation might alter, rather than simply reduce, the function of the splicing factor. We named this allele *prp8a-14*.

prp8a-14 improved *pex14-6* mRNA splicing, PEX14 protein accumulation, and peroxisome function

We examined the consequences of *prp8a-14* on *pex14-6* splicing. The *pex14-6* mutation in the last nucleotide (nt) of exon 1 changes the AG|gu consensus to AA|gu and disrupts splicing (Figure 2A; Burkhart et al., 2013). The major *pex14-6* mRNA derives from a cryptic ag|gu 5′-donor site 87-nt upstream of the normal 5′-splice site; splicing at this site removes exon 1 and part of the 5′-untranslated region (UTR; Figure 2A; Burkhart et al., 2013). This altered *pex14-6* transcript is 87-nt smaller than the wild-type transcript, a difference that we detected following agarose gel electrophoresis of cDNA amplified with primers spanning the excised region (Figure 2B). We isolated RNA from *pex14-6 prp8a-14* seedlings and reverse transcribed and PCR-amplified the affected region of the *pex14* transcript. Comparing these products to those from wild type and *pex14-6* revealed that the suppressor restored a wild-type-sized cDNA in *pex14-6* (Figure 2B). We sequenced this amplicon from the suppressor and found that splicing was now occurring at the mutated AA|gu 5′-splice site at the end of exon 1, which would restore the reading frame but change Glu25 to Lys in the resultant pex14 protein (Figure 2D).

The *pex14-6* mutant accumulates very low levels of protein detected by an anti-PEX14 antibody (Burkhart et al., 2013). Immunoblot analysis revealed that the suppressor largely restored pex14 protein levels (Figure 2C), confirming that *pex14-6* splicing was improved.

Despite the Glu25-to-Lys alteration in the pex14 protein accumulating in the suppressor, the mutated protein improved several peroxisome-related defects of *pex14-6*. PEX14 helps import peroxisomal enzymes from the cytosol into the organelle lumen. This import can be indirectly evaluated via immunoblot analysis of proteins that have their targeting sequences removed once inside the peroxisome, which results in a molecular weight difference between the intact cytosolic protein and the cleaved lumenal protein (Kao et al., 2018). One such protein is peroxisomal malate dehydrogenase (PMDH; Pracharoenwattana et al., 2007). We used immunoblotting to compare PMDH processing in wild-type, *pex14-6*, and *pex14-6 prp8a-14* seedlings and found that the suppressor increased PMDH cleavage in *pex14-6* (Figure 2C). This processing restoration suggested that lumenal protein import was improved.

We identified the *prp8a-14* allele based on its ability to restore IBA responsiveness to *pex14-6* roots (Figure 1A), and quantifying this phenotype confirmed improvement in peroxisome function. The *prp8a-14* mutation fully restored the ability of IBA to inhibit *pex14-6* root elongation in light-grown seedlings (Figure 2E). IBA also inhibits seedling stem

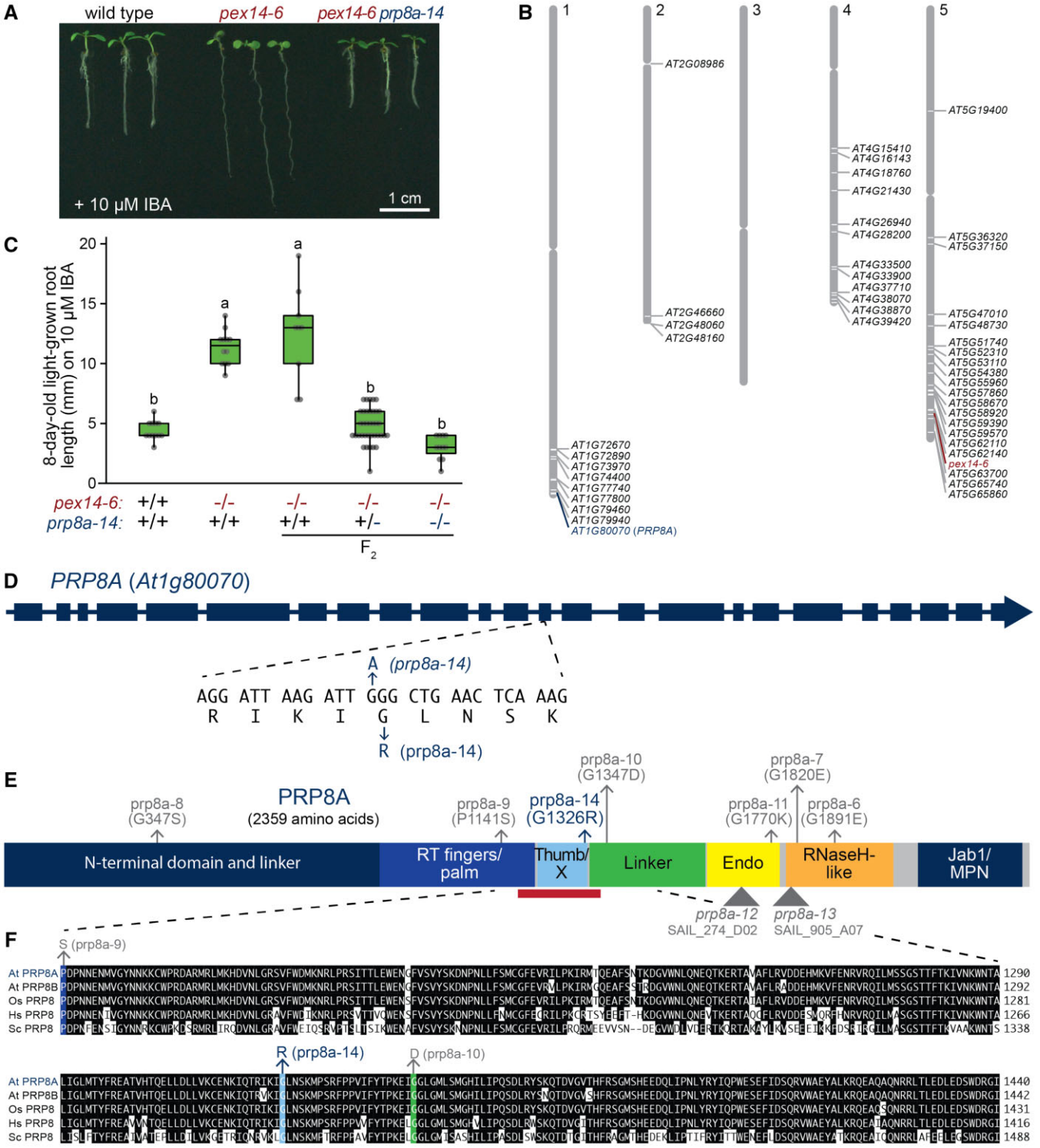

Figure 1 Identification of *prp8a-14* as a *pex14-6* suppressor. A, *pex14-6* suppressing mutants were isolated from a screen for restored sensitivity to the inhibitory effects of IBA on primary root growth as a proxy for restored peroxisome function. Representative seedlings grown for 8 days on 10-µM IBA were photographed. B, Whole-genome sequencing of one suppressor was used to identify mutations. The schematic of the five Arabidopsis chromosomes shows genes with homozygous nonsynonymous EMS-consistent mutations by gene ID number, including a missense mutation in *PRP8A*. C, *prp8a-14* suppression of *pex14-6* is semi-dominant. About 64 F_2 seedlings from the backcrossed suppressor were grown in the presence of 10 µM IBA along with wild-type and *pex14-6* controls, and roots were measured after 8 days. Each F_2 seedling was genotyped for the *prp8a-14* mutation and root lengths were plotted by genotype (+ , wild type; –, mutant). Boxes show second and third quartiles, horizontal lines are medians, and whiskers show the highest and lowest values within 1.5-fold of the interquartile range ($n > 12$). Data not sharing a letter above the boxplot are significantly different (one-way ANOVA with Tukey's post-hoc test, $P < 0.01$). D, Gene diagram of *PRP8A* with exons shown as rectangles, introns shown as connecting lines, and the *prp8a-14* missense mutation shown below the diagram. E, Protein schematic of PRP8A

(Continued)

(hypocotyl) elongation in dark-grown wild-type seedlings (Strader et al., 2011), whereas *pex14-6* hypocotyls elongate on IBA (Figure 2F; Burkhart et al., 2013). As with light-grown root elongation, *prp8a-14* fully restored IBA responsiveness to *pex14-6* hypocotyls (Figure 2F).

We also assessed *pex14-6* peroxisome function by monitoring seedling growth with and without supplemental fixed carbon. Until photosynthesis is established, seedlings rely on peroxisomal β-oxidation of stored seed fats for fixed carbon (reviewed in Graham, 2008). The peroxisomal defects of *pex14-6* limit growth on medium lacking fixed carbon (Figure 2F). Like other peroxisome-defective mutants (Hayashi et al., 1998; Zolman et al., 2000), *pex14-6* growth can be restored by the addition of a fixed carbon source (sucrose) to the growth media (Burkhart et al., 2013). Like IBA responsiveness, the *prp8a-14* mutation restored sucrose-independent hypocotyl elongation to dark-grown *pex14-6* seedlings (Figure 2F). Together, these physiological and molecular assays indicated that the *prp8a-14* mutant improved peroxisome function by correcting splicing in the *pex14-6* mis-splicing allele.

prp8a-14 restored splicing to only a subset of mis-spliced *pex14* transcripts

We have recovered a variety of *pex14* splice-site mutations from a range of peroxisome dysfunction screens (Monroe-Augustus et al., 2011; Burkhart et al., 2013; Fleming, 2016). To probe splice-site fidelity, we examined the ability of *prp8a-14* to suppress these mutants. Like in *pex14-6*, the mutated splice sites in *pex14-7*, *pex14-4*, and *pex14-12* (Figure 3A) confer peroxisome-defective phenotypes, including IBA-resistant and sucrose-dependent hypocotyl elongation in dark-grown seedlings (Figure 3, B–D), loss of full-length PEX14 protein (Figure 3, E–G), and reduced lumenal protein processing (Figure 3, E–G).

The *pex14-7* allele (Fleming, 2016) has a 5′-splice site G-to-A mutation analogous to *pex14-6*, changing a canonical AG|gu splice site to AA|gu in the last nucleotide of exon 5 (Figure 3A). We found that the spliceosome fails to recognize the mutated 5′-splice site of exon 5 and uses a cryptic 5′-splice site (GG|GU) 34-nt upstream in exon 5 (Figure 3A). This altered *pex14-7* transcript would encode seven out-of-frame amino acids starting at amino acid 226 followed by a stop codon (Supplemental Figure S1, A and B). We crossed *prp8a-14* to *pex14-7*, isolated RNA from the resultant double mutant, and amplified *pex14* cDNA using primers in exons 4 and 6 (Figure 3A; Supplemental Table S1). The *pex14-7* cDNA amplicon was smaller than the wild-type amplicon, whereas *pex14-7 prp8a-14* had a wild-type sized amplicon indicative of restored splicing (Figure 3H). We sequenced the major amplicon and confirmed restored splicing in the double mutant at the AA|gu site (Figure 3H; Supplemental Figure S1B).

This improved splicing in *pex14-7 prp8a-14* was accompanied by partially restored pex14 protein levels and improved PMDH processing (Figure 3E). Moreover, *pex14-7 prp8a-14* seedlings extended hypocotyls similarly with and without sucrose, unlike the sucrose-dependent elongation exhibited by *pex14-7* (Figure 3B). Similarly, IBA responsiveness was improved in the *pex14-7 prp8a-14* double mutant (Figure 3B). These phenotypic restorations suggest improved lumenal protein import and peroxisomal β-oxidation of fatty acids and IBA, implying that the pex14 protein in the double mutant, which would carry a Glu238-to-Lys mutation (Supplemental Figure S1B), remains functional.

Next, we tested *pex14-4*, which has a G-to-A mutation in the first nt of intron 8 (Monroe-Augustus et al., 2011). We found that this AG|gu-to-AG|au alteration results in skipping of exon 8 (Figure 3A), creating a frameshift with 24 out-of-frame amino acids starting at residue 293 followed by a stop codon (Supplemental Figure S1C). Analysis of cDNAs amplified using primers in exons 4 and 12 (Figure 3A; Supplemental Table S1) revealed exon 8 skipping not only in *pex14-4*, but also in *pex14-4 prp8a-14* (Figure 3I), indicating that *prp8a-14* did not restore *pex14-4* splicing. As expected from the persistence of this splicing defect, *prp8a-14* also did not restore PEX14 protein levels (Figure 3F), improve PMDH processing (Figure 3F), or restore IBA responsiveness or sucrose independence to *pex14-4* (Figure 3C).

To assess the ability of *prp8a-14* to impact 3′-splice-site selection, we monitored *pex14-12* (Fleming, 2016), which has a G-to-A mutation in the 3′-splice-acceptor site in the last nt of intron 11 (Figure 3A). We found that *pex14-12* transcripts were spliced at a cryptic 3′-splice site (AG|CG) 19-nt downstream of the mutated site (Figure 3A), which results in 78 frameshifted amino acids followed by a stop codon (Supplemental Figure S1D) and loss of full-length PEX14 protein (Figure 3G). We detected no splicing changes when we analyzed *pex14-12* transcripts with or without the *prp8a-14* mutation (Figure 3J). Accordingly, *pex14-12* defects in PEX14 protein levels (Figure 3G), PMDH processing (Figure 3G), growth without sucrose (Figure 3D), and IBA responsiveness (Figure 3D) were not restored by *prp8a-14*. We concluded that *prp8a-14* was able to restore splicing to only a subset of splice-site mutations.

Figure 1 (Continued)
functional domains (RT, reverse transcriptase; Th, thumb; Endo, endonuclease-like; MPN, Mpr1 Pad1 N-terminal) with the positions of various prp8a mutations indicated. The bar below the Th/X domain indicates the region that interacts with *U5* snRNA and the 5′ and branch point splice sites in yeast Prp8. F, Partial alignment of *A. thaliana* (At) PRP8A (At1g80070), and PRP8B (At4g38780) with homologs from *Oryza sativa* (Os; AAT07657.1), *Homo sapiens* (Hs; NP_006436.3) and *S. cerevisiae* (Sc; CAA80854.1) generated using the Clustal W method of the Megalign program (DNAStar). Amino acids identical in at least three proteins are in white text. The positions of selected prp8a missense alleles are indicated above the alignment.

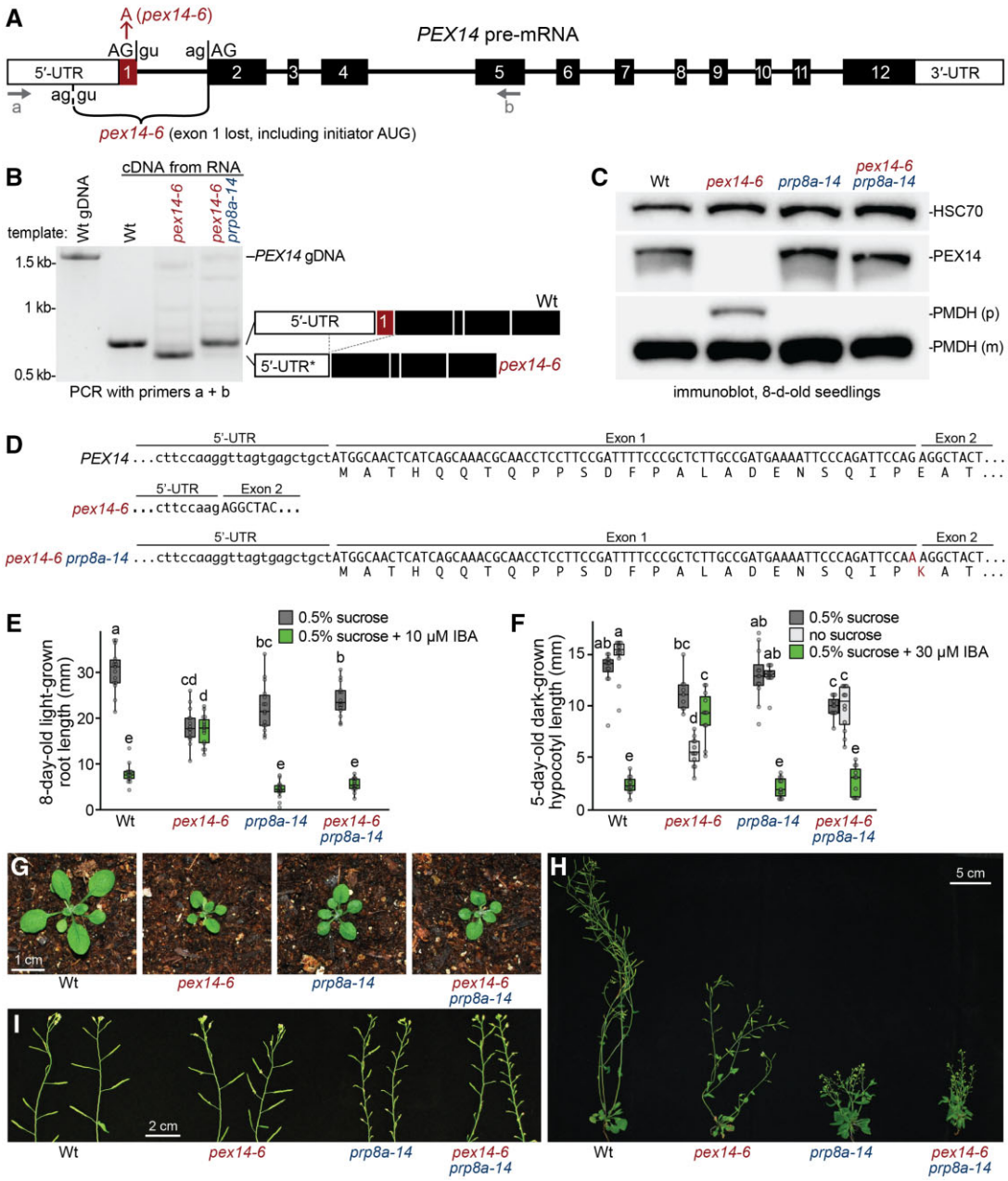

Figure 2 *prp8a-14* improves *pex14-6* splicing, restores PEX14 protein accumulation, and improves peroxisome-related physiological functions. A, Pre-mRNA diagram of *PEX14* showing alternative splicing observed in *pex14-6* and primers used for cDNA amplification (horizontal arrows). Noncoding nucleotide residues are in lower case. B, *prp8a-14* restores *pex14-6* splicing. Electrophoresis of cDNA amplified from seedling RNA using primers shown as horizontal arrows in (A). The major amplicons were excised and sequenced, and the observed splicing products are depicted to the right of the corresponding amplicons. C, *prp8a-14* restores pex14 protein accumulation in *pex14-6*. Protein extracts from 8-day-old light-grown seedlings were processed for immunoblotting with the indicated antibodies. Mature (m) PMDH is synthesized as a precursor (p) that has its targeting sequence removed after peroxisomal import. Heat shock cognate 70 (HSC70) is a cytosolic loading control. D, Sequences of spliced transcript encompassing the *pex14-6* mutation from wild-type, *pex14-6*, and *pex14-6 prp8a-14* cDNAs shown above the predicted protein sequences. Note the E25K missense mutation in the correctly spliced *pex14-6* transcript in the *pex14-6 prp8a-14* mutant. Exon sequences are capitalized, and UTR sequences are in lower case. E, *prp8a-14* increases IBA responsiveness in light-grown *pex14-6* seedlings. Root lengths of 8-day-old seedlings grown at 22°C under continuous, yellow-filtered light are shown ($n > 12$). Boxes show second and third quartiles, horizontal lines are medians, and whiskers show the highest and lowest values within 1.5-fold of the interquartile range. Data not sharing a letter above the boxplot are significantly different (one-way ANOVA with Tukey's post-hoc test, $P < 0.01$). F, *prp8a-14* increases IBA responsiveness and restores sucrose independence in dark-grown *pex14-6* seedlings. Hypocotyl lengths of 5-day-old seedlings grown in the dark on the indicated media at 22°C are shown ($n > 9$). Boxes show second and third quartiles, horizontal lines are medians, and whiskers show the highest and lowest values within 1.5-fold of the interquartile range. Data not sharing a letter above the boxplot are significantly different (one-way ANOVA with Tukey's post-hoc test, $P < 0.01$). G–I, *prp8a-14* has small rosettes (G), reduced stature (H), and reduced fertility and internode elongation (I). Seedlings germinated on plant nutrient media with 0.5% sucrose were transferred to soil and representative plants (G, H) or inflorescence stems (I) were photographed at 19 (G), 39 (H), or 52 (I) days after sowing.

Global impacts of the *prp8a-14* mutation on development, transcript levels, and splicing

The *prp8a-14* single and double mutants displayed reduced fertility along with small stature due to reduced leaf expansion (Figure 2G) and shortened inflorescence stems (Figure 2, H and I). These morphological defects suggested that the *prp8a-14* mutation caused transcript changes beyond altered *pex14* splicing. To explore the impact of *prp8a-14* on transcript levels and splicing, we prepared RNA from three biological replicates of 8-day-old wild-type and *prp8a-14* seedlings and conducted RNA-seq analysis. Each sample yielded between 28.2 million and 36.2 million paired-end reads, of which 97.5%–97.7% mapped to The Arabidopsis Information Resource (TAIR)10 Arabidopsis reference genome. Out of 26,896 transcripts detected, 7,241 had significantly different abundance in *prp8a-14* seedlings, including 784 with at least two-fold lower levels and 246 with at least two-fold higher levels (Supplemental Data Set 1; Figure 4A). Both *PRP8A* and *PEX14* mRNAs were present at similar levels in wild-type and *prp8a-14* seedlings (Supplemental Data Set 1).

We monitored enriched gene ontology (GO) terms among differentially expressed genes in our dataset. Transcripts downregulated more than two-fold in *prp8a-14* were significantly enriched for responses to sulfur starvation and triterpenoid metabolism GO terms (Figure 4B), and RNA processing, gene expression, and root development GO terms were enriched among all genes significantly downregulated (Supplemental Figure S2A). Transcripts upregulated more than two-fold were enriched in multiple GO terms involving seed and reproduction processes (Figure 4C), whereas RNA processing, photosynthesis, pigment biosynthesis, and postembryonic development GO terms were enriched among all genes significantly upregulated (Supplemental Figure S2B).

Because the *prp8a-14* mutant altered splicing in *pex14-6* (Figure 2) and *pex14-7* (Figure 3), we assessed the global consequences of the *prp8a-14* mutation on splicing by analyzing splice junctions in our RNA-seq data. We quantified intron retention, exon skipping, and use of alternative 5′- and 3′-splice-site events in wild type and *prp8a-14* (Supplemental Data Set 2). Consistent with previous findings (Wang and Brendel, 2006; Marquez et al., 2012), intron retention was the most common (5,475, 41.5%) alternative splicing event among 13,177 alternative splicing events detected in wild type and *prp8a-14* (Figure 5A). No additional alternative splicing events were detected in *prpr8a-14* that were not also present in wild type. We compared the frequency of alternative splicing events between wild type and *prp8a-14*. Of all alternative splicing events detected, 684 (5.2%) were significantly differentially spliced in *prp8a-14* compared to wild-type (Figure 5A). Genes with significantly different splicing in *prp8a-14* were enriched for GO terms involving regulation of circadian rhythm and several regulatory processes (Figure 5B).

Among alternative splicing events detected, only ∼2% of the intron retention (139/5475) or exon skipping (77/3213) events were significantly different in *prp8a-14* (Figure 5A). In contrast, 10% of the detected alternative 5′- (200/1844) and 3′- (268/2645) splice-site events were significantly different in *prp8a-14* and wild type (Figure 5, A and C), hinting that the mutation impacted splice-site selection more than the decision to remove an intron or skip an exon. Indeed, hypergeometric testing supports a significant *prp8a-14* enrichment of differentially spliced 5′- and 3′-splice-site events ($P < 0.0001$), but not of intron retention or exon skipping events. In addition, *prp8a-14* appeared to favor the splice site closest to the branch site (Figure 5A). Specifically, 60% (119/200) of the altered 5′-splice sites favored the closer site in *prp8a-14* ($P = 0.007$, two-tailed *z* test compared to a 1:1 ratio). Similarly, 73% (195/268) of altered 3′-splice sites favored the closer site in *prp8a-14* ($P < 0.0001$, two-tailed *z* test compared to a 1:1 ratio).

We generated sequence logos to visualize preferred sequence motifs at the 1,844 5′-splice sites with alternate splicing events. As expected, the intronic +1 (g) and +2 (t) positions of the AG|gt 5′-splice-site motif were highly preferred, whereas the exonic −1 (G) and −2 (A) positions were less preferred. Splice sites preferred by wild type and *prp8a-14* were similar (Figure 5D; Supplemental Figure S3A, top row). In the 200 junctions in which *prp8a-14* and wild type had an at least 5 percentage point difference in 5′-splice-site selection, we found a significant decrease in the preference for the exonic −1 G and a significant increase in the preference for −1 A in the *prp8-14* mutant (Figure 5D; Supplemental Figure S3A, middle row, $P = 0.046$, two-sample Chi-square test). This difference was further exaggerated when we limited the analysis to the 92 junctions where wild type and *prp8a-14* differed by at least 20 percentage points (Figure 5D; Supplemental Figure S3A, bottom row, $P < 0.0001$, two-sample Chi-square test), indicating that the *prp8a-14* mutation reduced the preference for a G at this position. In contrast, the splice-site motifs between alternatively spliced 3′-splice sites appeared similar in wild type and *prp8a-14* (Supplemental Figure S3B).

Altered splicing can lead directly to changes in transcript levels (e.g. nonsense-mediated decay) or can change transcript levels indirectly through impacts of alternative splicing on regulatory networks. To investigate the possible impact of altered splicing in *prp8a-14* on transcript levels, we compared our genes with differentially spliced transcripts with our genes with altered transcript levels. We did not find significant enrichment of differentially expressed genes among our differentially spliced transcripts (Figure 5A), suggesting that the altered splicing that we detected was not robustly impacting transcript levels.

BRR2, named after the yeast Bad response to refrigeration 2 (Brr2) protein, is a spliceosomal helicase that directly interacts with PRP8 (Nguyen et al., 2013). Like *prp8a-14*, the *brr2a-2* mutant has a compact rosette and small siliques (Mahrez et al., 2016). This mutant has been subject to RNA-seq analysis in 15-day-old seedlings, and transcripts with differential intron retention in the mutant are annotated (Mahrez et al., 2016). We found minimal overlap between

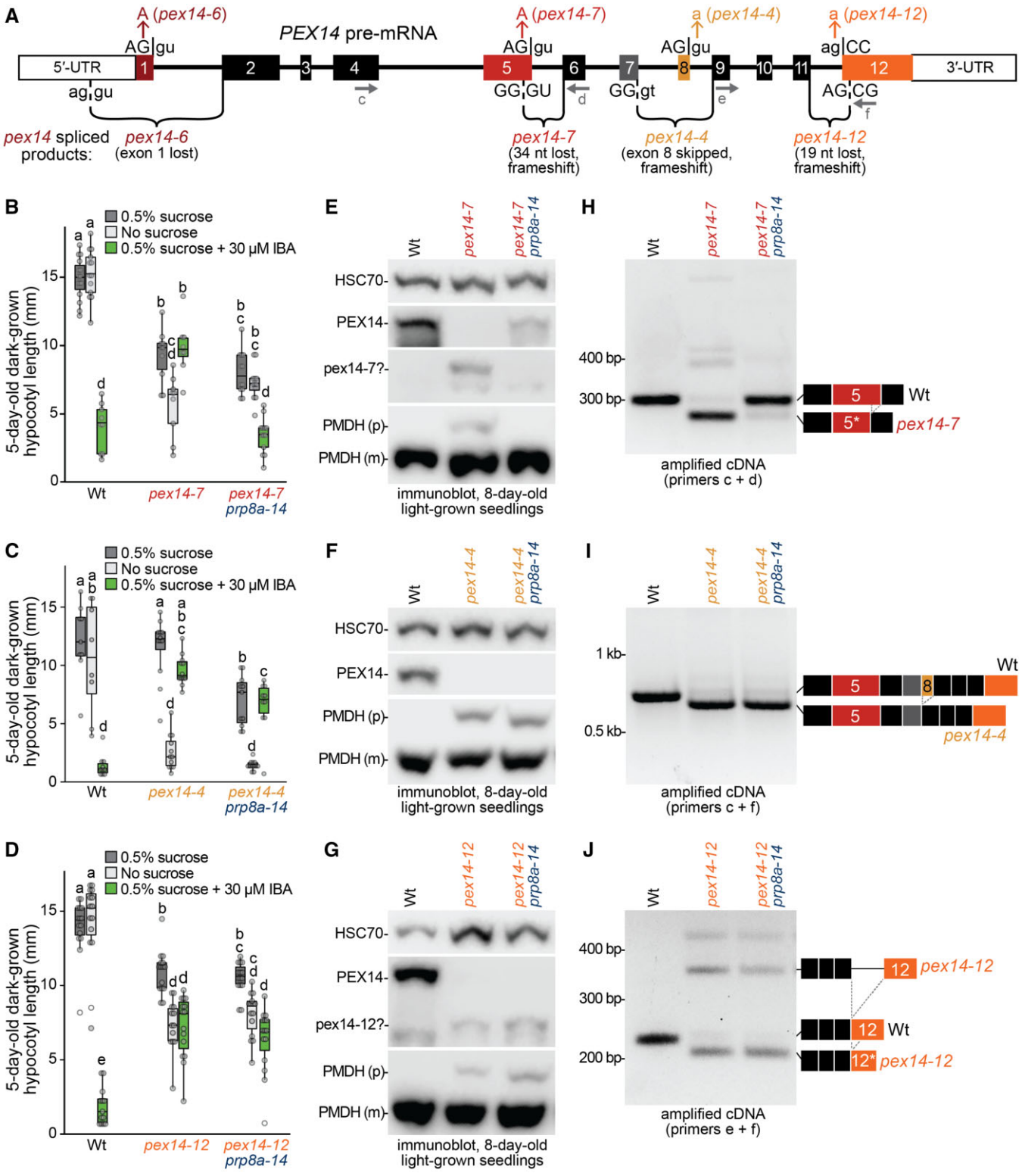

Figure 3 *prp8a-14* restores splicing and pex14 protein to a subset of *pex14* mis-splicing alleles. A, Pre-mRNA diagram of *PEX14* showing alternative splicing observed in selected *pex14* alleles and primers used for cDNA amplification (horizontal arrows). Noncoding nucleotide residues are in lower case; B–D, Hypocotyl lengths of 5-day-old seedlings grown in the dark on the indicated media reveal that *prp8a-14* restores sucrose-independence and IBA responsiveness of *pex14-7* (B) whereas *prp8a-14* does not change IBA responsiveness or sucrose dependence of *pex14-4* (C) or *pex14-12* (D). Boxes show second and third quartiles, horizontal lines are medians, and whiskers show the highest and lowest values within 1.5-fold of the interquartile range ($n > 8$). Data not sharing a letter above the boxplot are significantly different (one-way ANOVA with Tukey's post-hoc test, $P < 0.01$). E–G, Immunoblots of protein extracted from 8-day-old seedlings and probed with the indicated antibodies reveal that *prp8a-14* restores pex14 protein accumulation and PTS2 processing to *pex14-7* (E), but not *pex14-4* (F) or *pex14-12* (G). p, precursor; m, mature; H–J, cDNA amplified from seedling RNA using the indicated primers and separated using agarose electrophoresis reveals that *prp8a-14* restores *pex14* splicing to *pex14-7* (H), but not *pex14-4* (I) or *pex14-12* (J). The major amplicons were excised and sequenced, and the observed splicing products are depicted to the right of the corresponding amplicons.

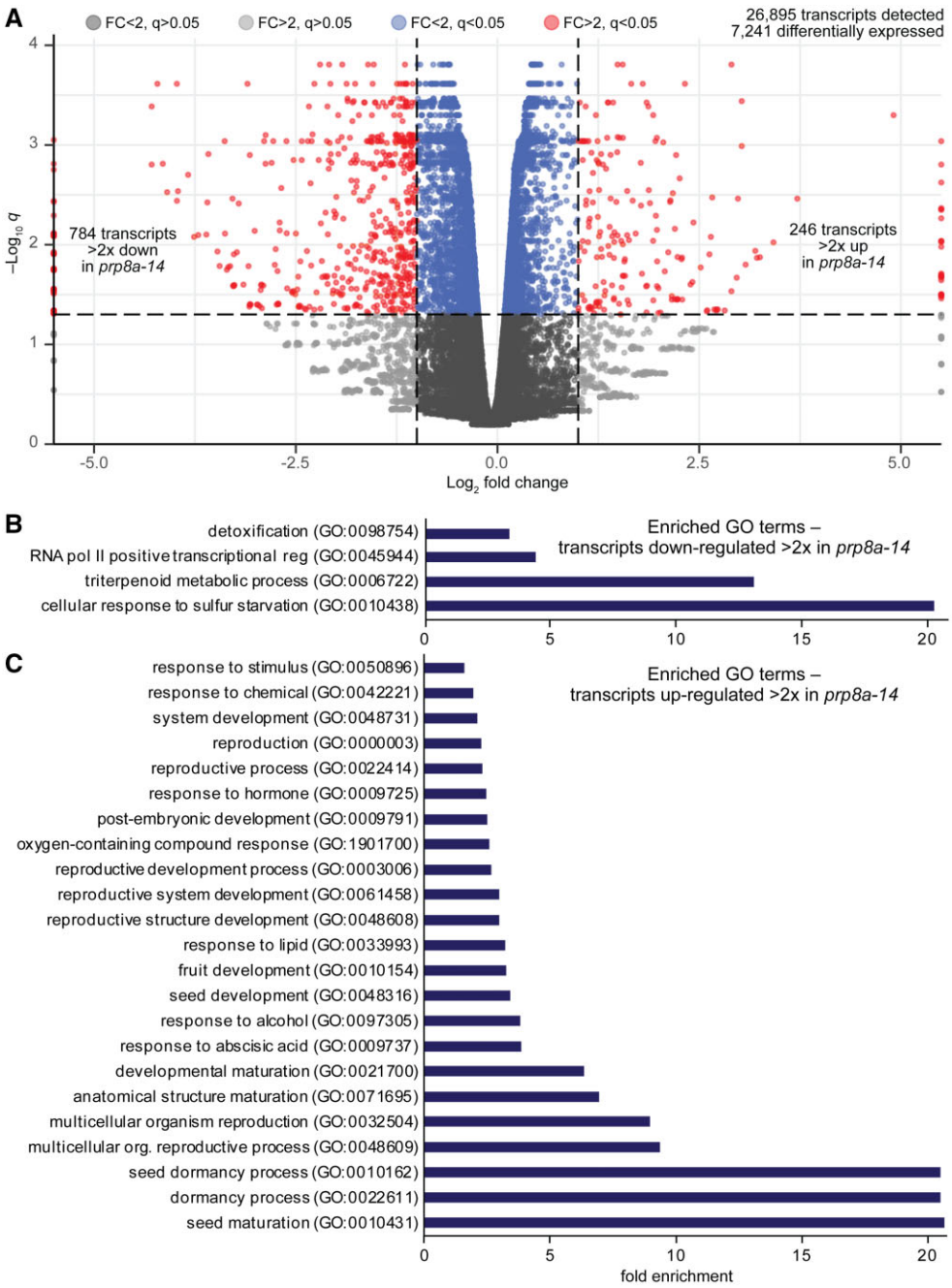

Figure 4 Thousands of genes are differentially expressed in *prp8a-14*. A, Summary of transcript accumulation in *prp8a-14* compared to wild type. The volcano plot was generated using the EnhancedVolcano package in R. Of the 26,895 transcripts detected (Supplemental Data Set 1), levels of 7,241 transcripts were significantly altered in *prp8a-14* ($q < 0.05$) (points above horizontal dashed line). Transcripts altered at least two-fold are in red (246 increased and 784 decreased). B, Enriched GO terms ($q < 0.05$) for genes with transcripts down at least two-fold in *prp8a-14*. C, Enriched GO terms ($q < 0.05$) for genes with transcripts up at least two-fold in *prp8a-14*.

brr2a-2 and *prp8a-14* transcripts with increased or decreased intron retention. Only two genes, *At2g34450* and *At3g09540*, displayed increased retention of an intron in both mutants; no genes with decreased intron retention were shared. In addition, we compared differentially accumulating transcripts in *prp8a-14* and *brr2a-2* to determine whether similar pathways were misregulated (Supplemental Data Set 3). We found significant overlap (hypergeometric test, $P < 0.0001$) between commonly upregulated (73) and downregulated (41) genes (Supplemental Figure S4). The common upregulated genes were enriched for GO terms involved in circadian rhythm and light responses, whereas shared downregulated genes were enriched for defense and immune response (Supplemental Figure S4).

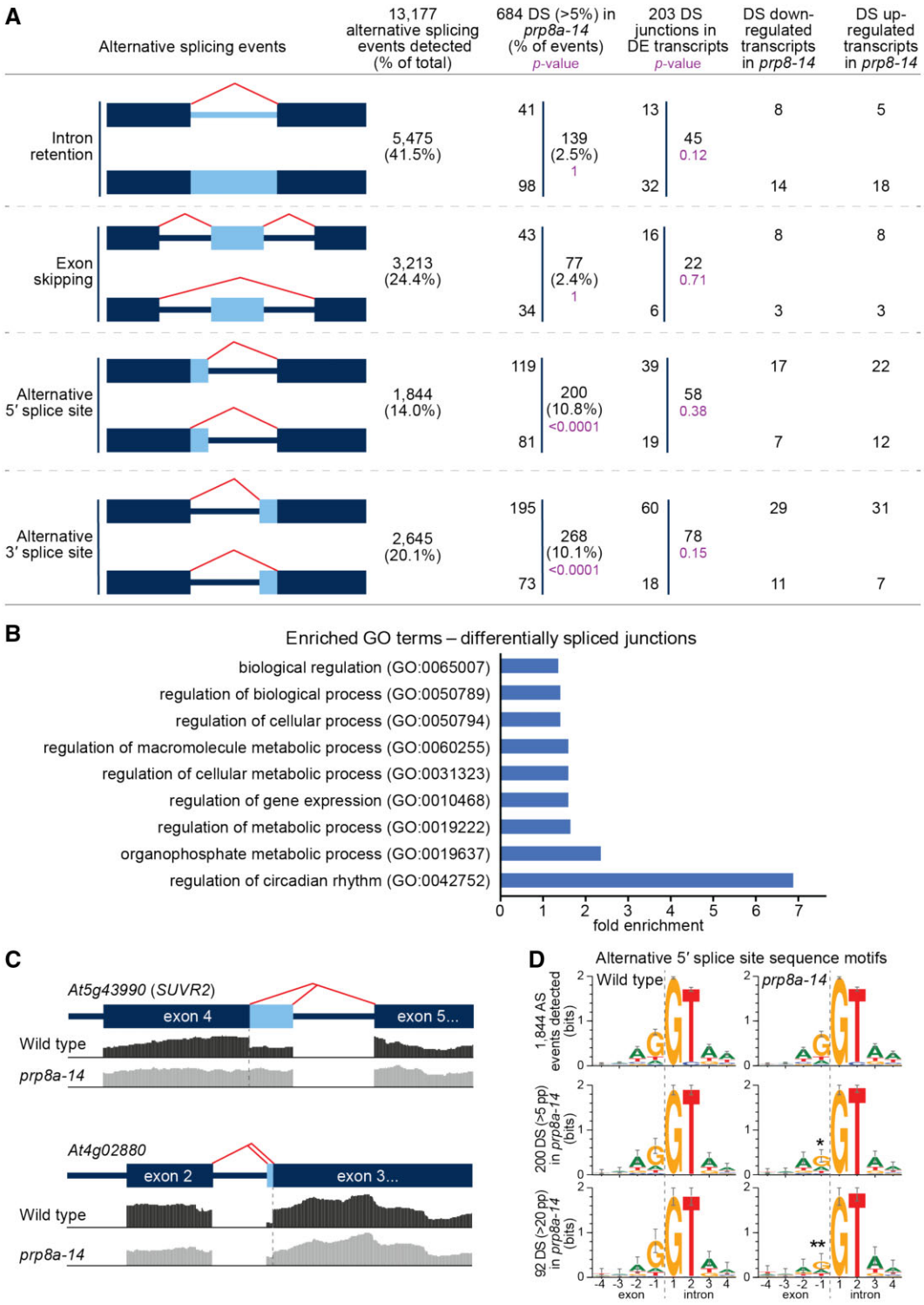

Figure 5 *prp8a-14* altered 5′- and 3′-splice-site selection. A, Summary of splicing in *prp8a-14* compared to wild type. rMATS was used to detect altered splice junctions in RNA-seq data from 8-day-old light-grown seedlings. Schematics illustrate four categories of alternative splicing events; rectangles depict exons, thick (blue) lines depict introns, and thin (red) lines highlight alternative splicing of light blue regions. Significantly different splicing (DS) events in *prp8a-14* were tabulated and further subtotaled by *prp8a-14* splicing preference. DS events in *prp8a-14* differentially expressed (DE) transcripts are tabulated. Hypergeometric testing *P*-values are shown in purple; $P < 0.05$ indicates significant enrichment. B, Enriched GO terms ($q < 0.05$) for genes with differential splicing events in *prp8a-14*. C, Examples of alternatively spliced junctions that were differentially spliced in wild type and *prp8a-14* illustrated by plotting RNA-seq reads using IGV spanning an impacted 5′- (top) or 3′-splice site in the indicated genes. D, Sequence logos generated using WebLogo 3 of preferred wild-type and *prp8a-14* 5′-splice-site sequence motifs for all 1,844 5′-alternative splicing events (top row), the 200 junctions with significantly DS (>5 percentage points [pp]) between *prp8a-14* and wild type (middle row), and the 92 junctions with significantly DS (>20 pp) between *prp8a-14* and wild type (bottom row). Error bars indicate approximate Bayesian 95% confidence intervals. Asterisks indicate significant differences from wild type (*$P < 0.05$; **$P < 0.0001$; two-sample Chi-squared test).

Discussion

Accurate mRNA splicing requires precise recognition of sequences that define the 5′, 3′, and branch point splice sites. We used *pex14-6*, a peroxisome-defective mutant with reduced protein accumulation due to mis-splicing of the first exon (Figure 2A), in a suppression screen for restored peroxisome function. We recovered a mutant in the PRP8A splicing factor that corrected *pex14-6* splicing, restored pex14 protein accumulation, and improved peroxisome function. PRP8 is a permanent component of the U5 snRNP that scaffolds pre-mRNA positioning within the spliceosome by interacting with four regions on the pre-mRNA to define which section to remove (reviewed in Siatecka et al., 1999). PRP8 also interacts with other permanent and transient proteins that usher the spliceosome as it cycles through the different conformations to remove an intron. To analyze the extent of suppression, we employed an allelic series of splice-site mutations in *PEX14*, which encodes a protein that assists the import of proteins into the peroxisome lumen (Azevedo and Schliebs, 2006). *prp8a-14* improved *pex14* splicing and rescued the peroxisome-defective phenotypes of *pex14-6* and *pex14-7* but not *pex14-4* or *pex14-12*. Thus, only *pex14* alleles with mutations in the exonic G of the 5′-splice site (AG|gu to AA|gu) were suppressed by *prp8a-14*.

Arabidopsis *prp8* mutants

Arabidopsis PRP8A is essential for embryogenesis, and *prp8a* null alleles confer embryo lethality (Schwartz et al., 1994; Marquardt et al., 2014; Sasaki et al., 2015; Deng et al., 2016; Kulichová et al., 2020). Two of the previously described viable *prp8a* missense alleles, *prp8a-6* and *prp8a-7* (Figures 1, E and 6, B), are hypomorphs that are late flowering and display increased intron retention (Marquardt et al., 2014; Sasaki et al., 2015). The developmental impacts of other *prp8a* missense mutations (*prp8a-8*, *prp8a-9*, *prp8a-10*, and *prp8a-11*; Figures 1, E and 6, B) have not been reported. Our viable *prp8a* missense mutant exhibits pleiotropic defects, including reduced fertility and small stature (Figure 2, G and H) that are perhaps unsurprising given the dramatic repercussions that even small changes in splicing can have on protein production.

Global analysis of mRNA splicing in *prp8a-14* showed significant differences from wild type at only a small subset of splicing junctions. Strikingly, we did not detect alternative splicing events in *prp8a-14* that were not also detected in wild type. This result indicates that *prp8a-14* did not markedly reduce splicing efficiency, which would presumably increase intron retention and/or exon skipping. Instead, the alternatively spliced junctions that were altered in *prp8a-14* were enriched for those showing differential splicing of 5′- and 3′-splice sites (Figure 5A). Among these differentially spliced junctions, *prp8a-14* often favored the site closest to the branch site, thus shortening the intron in both the 5′- and 3′-splice sites (Figure 5, A and C). Indeed, in both *pex14* mutants suppressed by *prp8a-14*, the *prp8a-14* mutant favored a splice site closer to the branch site (Figures 2, B and 3, H). In contrast, intron retention and exon skipping events were not significantly enriched in *prp8a-14* versus wild type (Figure 5A). This disproportionate alteration of 5′- and 3′-splice sites among detected alternative splicing events suggests that the *prp8a-14* mutation modulates splice-site selection without markedly affecting excision and ligation of RNA substrates, which would be consistent with a role for PRP8a in alternative splicing. Moreover, analysis of splice-site motifs of differentially spliced junctions suggests that *prp8a-14* relaxes fidelity at the −1 position of 5′-splice sites (Figure 5D). Interestingly, both *pex14* mutations that were suppressed by *prp8a-14* carry mutations at the −1 position of 5′-splice sites (Figures 2 and 3).

The first reported viable missense mutation of *PRP8A*, *prp8a-6*, was isolated for its impact on *FLOWERING LOCUS C* (*FLC*, *At5g10140*) expression due to altered splicing of the anti-sense transcriptional regulator *COOLAIR* (*At5g01675*; Marquardt et al., 2014). The *prp8a-6* mutation (Figures 1, E and 6, B) increases *FLC* expression, which delays flowering (Marquardt et al., 2014). *COOLAIR* and *FLC* had the largest relative decreases in transcript levels in *prp8a-14* (Supplemental Data Set 1). However, these genes did not emerge from our analysis of genes differentially spliced in *prp8a-14* (Supplemental Data Set 2), perhaps because transcript levels were very low in the mutant: *COOLAIR* transcript was undetected in two of three *prp8a-14* biological replicates and *FLC* was undetected in one replicate (Supplemental Data Set 1). Analysis of transcripts from older plants might increase detection of *FLC* and *COOLAIR* transcripts to allow analysis of any splicing alterations in *prp8a-14*.

Although *prp8a-14* has a compact rosette, small siliques, and short inflorescence stems (Figure 2, G–I), GO enrichment analysis of transcripts that differentially accumulated (Figure 4, B and C) or were differentially spliced (Figure 5B) in *prp8a-14* seedlings did not reveal terms that were obviously related to rosette architecture. Investigation of RNA from adult tissues might illuminate specific transcriptional or splicing changes that are driving these *prp8a-14* phenotypes. Adult morphological phenotypes are not reported for the other Arabidopsis *prp8a* alleles; however, the small stature of *prp8a-14* resembles *brr2a-2* (Mahrez et al., 2016), a mutant of the helicase that interacts with PRP8 to activate the spliceosome for the first catalytic step (Nguyen et al., 2013). We found significant overlap in genes upregulated or downregulated in both mutants (Supplemental Figure S4). For example, both *prp8a-14* (Supplemental Data Set 1) and *brr2a-2* seedlings (Mahrez et al., 2016) have reduced *FLC* transcript levels. We did not find substantial overlap in transcripts with altered intron retention in the two mutants, however, and informative comparison of this and other splicing parameters would require a direct assessment using RNA from age- and growth condition-matched samples.

Arabidopsis prp8a-14 may impact the second step of splicing

Extensive suppression studies in yeast have established a critical role for Prp8 in spliceosome splice-site recognition

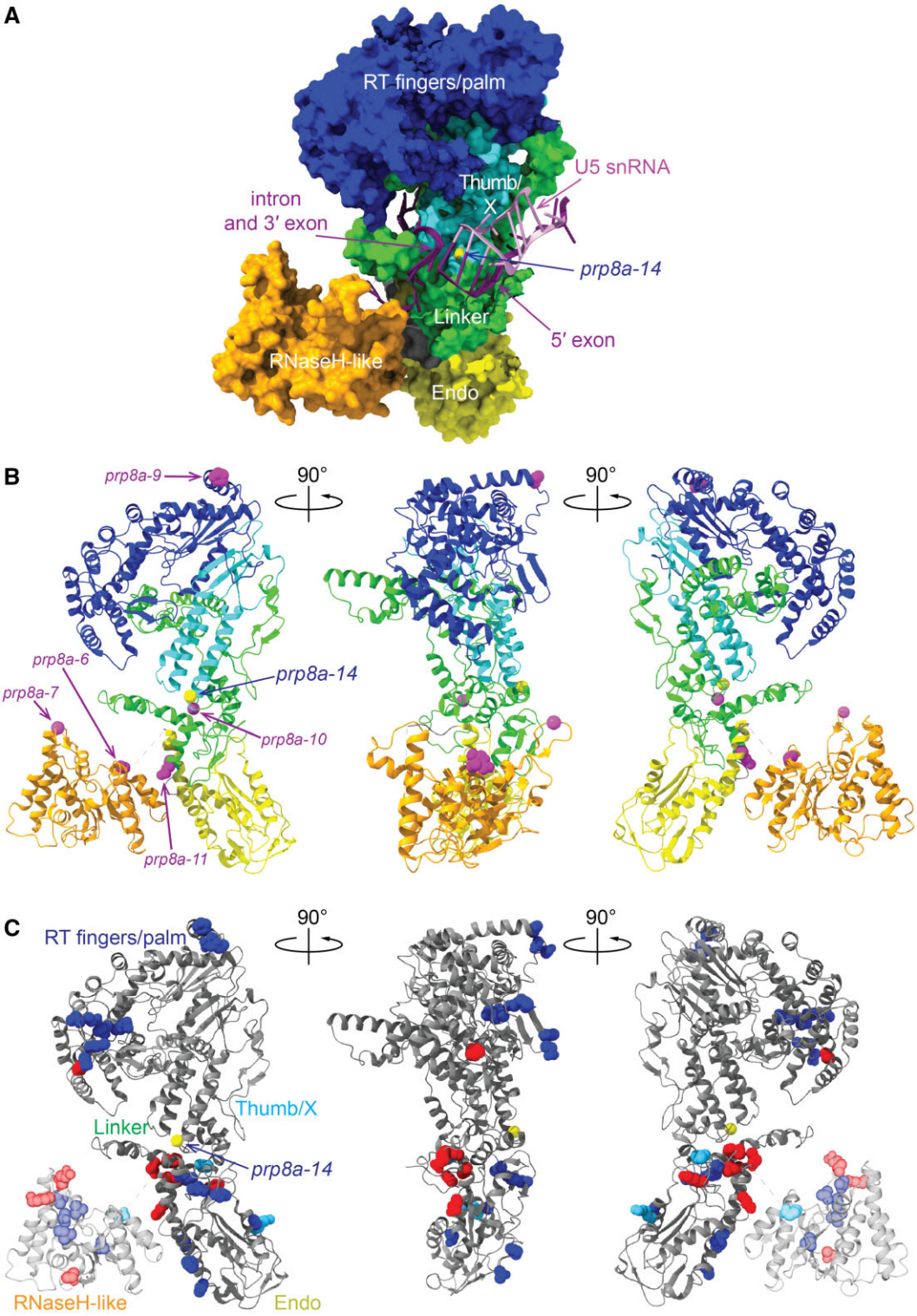

Figure 6 Predicted position of residue altered in Arabidopsis prp8a-14 based on the crystal structure of the related *S. cerevisiae* Prp8 in the C* complex spliceosome. A, Surface model of PRP8 of RT (reverse transcriptase)/palm through RNase-H like domains rendered from PDB 5WSG using ChimeraX (Yan et al., 2017) colored as annotated in Figure 1E. The *U5* snRNA is shown in lavender, pre-mRNA 5′-exon and 3′-intron/exon are in purple, and the altered residue in *prp8a-14* is in yellow. B, Ribbon model of *S. cerevisiae* Prp8 colored as in (A) and rotated 90° with altered residues corresponding to *prp8a-14* shown in yellow and other Arabidopsis missense alleles shown in magenta. C, Ribbon models of *S. cerevisiae* Prp8 rotated 90° with Arabidopsis *prp8a-14* in yellow and *S. cerevisiae* suppressors discussed in the text in blue (step-one suppressors) or red (step-two suppressors). Step-one suppressors confirmed using mutated pre-mRNA are shown in light blue (Liu et al., 2007). The RNase-H-like domain was removed from the center panel to more clearly show clustered first- and second-step suppressors in the Endo domain.

and fidelity (Liu et al., 2007; Galej et al., 2013). To examine the role of yeast Prp8 in splice-site recognition, pre-mRNA reporters mutated at different locations in the 5′, 3′, or branch point splice sites were used to monitor pre-mRNA processing in various *prp8* mutants (Collins and Guthrie, 1999; Siatecka et al., 1999; Ben-Yehuda et al., 2000; Query and Konarska, 2004; Liu et al., 2007). The *prp8* first-step alleles restore splicing to splice-site mutations that block the first trans-esterification reaction (characterized by reduced levels of both lariat and fully spliced transcript), whereas second-step alleles restore splicing to splice-site mutations that stall after the first trans-esterification reaction (characterized by lariat presence but reduced levels of fully spliced transcript) (Figure 6C; Query and Konarska, 2004; Liu et al., 2007). Improvements in either the first or second step are mutually exclusive, which led Query and Korsanka to develop the two-state model of splicing. In this model, the spliceosome alternates between conformations favoring the first or second step, and mutations that disrupt this equilibrium impair splicing (Query and Konarska, 2004).

Our *prp8a-14* mutant resembles the yeast second-step alleles. Only second-step alleles fully splice the 5′- and 3′-mutations tested in yeast (Liu et al., 2007). Thus, *prp8a-14* restoration of fully spliced transcripts in our 5′-splice-site AG|gu-to-AA|gu *pex14-6* and *pex14-7* mutations implies a second-step allele. Further supporting second-step classification is the location of our *prp8a-14* mutation. Examination of the yeast Prp8 structure in the C* spliceosome conformation (Yan et al., 2017) reveals that the prp8a-14 G1326R mutation is in the Thumb/X subdomain between the reverse transcriptase fingers/palm (RT) and endonuclease (En) domains at the center of the active site in the concave surface facing the RNaseH-like domain (Figure 6). Several yeast second-step alleles are located along the same surface in the RT/En domain surrounding the active site facing the RNaseH-like domain (Figure 6C; reviewed in Galej et al., 2013). In contrast, the yeast first-step alleles, excluding those on the RNaseH-like domain, reside along the outer-facing surfaces of Prp8 (Figure 6C; reviewed in Galej et al., 2013). Definitive classification of *prp8a-14* as a second-step allele could be provided by examining *prp8a-14* effects on additional splice-site mutations analogous to those tested in yeast.

Failure to complete the second catalytic reactions in *pex14-6* and *pex14-7* might result from altered base-pairing with the substrate RNA in the active site. The predominant transcript in both *pex14* alleles used a cryptic 5′-splice-site upstream of normal splice site. However, the improved splicing that we observed in the suppressor implies that some correctly cleaved intron lariat accumulated. The 5′-AA|gu mutations in *pex14-6* and *pex14-7* do not alter the lariat sequence and are expected to keep wild-type configurations with *U2* and *U6* snRNA (Wan et al., 2016). However, the additional adenine on the end of the exon might form a conventional A:U pairing with a uracil on the end of *U5* loop 1, rather than the G:U wobble pairing of wild type. This altered pairing might stabilize the exon in the active site and inhibit repositioning of the spliceosome or ligation with the 3′-splice site, eventually triggering complex destabilization and lariat degradation. Indeed, mutated yeast 5′- and 3′-pre-mRNA reporters display elevated lariat intermediate levels when degradation is inhibited (Liu et al., 2007). Our *prp8a-14* mutation (G1326R) is in the Thumb/X domain in the spliceosome active site that binds the end of the 5′-exon and the *U5* loop (Figure 6A; reviewed in Galej et al., 2013). Perhaps the ectopic arginine restores RNA substrate active site interaction to favor ligation with the 3′-exon, saving the transcript from degradation.

The *pex14-4* allele (AG|gu to AG|au) was the only pre-mRNA mutation we tested with an analogous mutation in the yeast studies. This +1 intron position is one of only two 5′-positions that are not suppressed by a yeast second-step *prp8* allele (Collins and Guthrie, 1999; Siatecka et al., 1999; Query and Konarska, 2004). Similarly, this allele was not rescued in our assays (Figure 3, C, F, and I). Because accumulation of lariat intermediate in the yeast studies of this position (Query and Konarska, 2004) suggests a capacity to be rescued by a second-step allele, failure to restore splicing implies the +1 intron position is critical for the second reaction in yeast. In Arabidopsis, nearly 5% of spliced junctions use the minor U12-containing spliceosome and remove |at-ac| introns rather than the canonical |gt-ag| introns processed by the predominant U2-containing spliceosome (Marquez et al., 2012). Although the *pex14-4* mutation changes the 5′-splice site of intron 8 to match the U12 consensus, the 3′-ag| splice site likely prevents U12-mediated splicing at this mutated site.

Our *prp8a-14* allele also failed to restore splicing to a 3′-splice-site mutation (ag|CC to aa|CC) in *pex14-12* (Figure 3, D, G, and J). In yeast, second-step *prp8* alleles do rescue splicing defects of several 3′-splice-site mutations, including a change to cytosine in the same position as *pex14-12* (Collins and Guthrie, 1999). However, the ag|CC 3′-splice site in *PEX14* that we tested is not canonical (ag|GU), and the *pex14-12* mutation to aa|CC may render the site unrecognizable. Indeed, yeast *prp8* does not restore splicing if both guanines in the 3′-splice site are changed to cytosines (Query and Konarska, 2004). Testing changes to a canonical 3′-splice site could clarify if our *prp8a* mutant is capable of the range of suppression seen in yeast second-step *prp8* alleles.

Although in-depth yeast studies have elucidated the relationship between Prp8 and pre-mRNA sequence, the impact of changes to the exonic guanine in the −1 position of the 5′-splice site was not explored. In yeasts, this guanine is not critical for splice-site recognition (Lesser and Guthrie, 1993). However, this guanine is highly conserved in mammals and plants and, along with the following intronic guanine, defines the exon–intron boundary during splicing in humans (Aebi et al., 1987; Galej, 2018). Further investigation of the relationship between the exonic guanine and the spliceosome may elucidate critical components of the spliceosome

in multicellular organisms. Of particular interest would be elucidation of components or mechanisms for alternative splicing, which is limited in yeast but plays important roles in plant and animal development.

pex mutants provide a convenient platform for genetic dissection of splicing specificity

Most viable Arabidopsis *prp8a* missense mutations, including our allele, were isolated in investigations of biological processes other than splicing using suppression screens that were (unknowingly) sensitized to detect altered splicing (Marquardt et al., 2014; Sasaki et al., 2015; Deng et al., 2016; Kulichová et al., 2020). Similarly, several yeast *prp8* alleles were isolated in suppression screens (Galej et al., 2013).

Unlike the pre-mRNA mutations probed in the yeast studies, which were specifically developed to report measuring splicing efficiency (Lesser and Guthrie, 1993), the alleles we used were genomic mutations recovered from screens for peroxisome-defective mutants. Our lab has accumulated an extensive collection of splice-site mutants because the mutagen used (EMS) alters guanine base-pairing during replication to cause G-to-A mutations (Greene et al., 2003). Thus, the splice-site consensus sequences AG|gt and ag|GT, each with two guanines, are particularly vulnerable to EMS mutagenesis. Splice-site mutations disrupt translation, resulting in drastic effects on protein production. Of sixteen *PEX14* alleles recovered from a range of peroxisome dysfunction screens (Monroe-Augustus et al., 2011; Burkhart et al., 2013; Fleming, 2016), half are splice-site mutants. Because PEX14 is important but not essential for peroxisome protein import (Monroe-Augustus et al., 2011), null *pex14* alleles, including splice-site mutations, disrupt peroxisome function without conferring lethality, resulting in easily monitored physiological phenotypes that are reversed when splicing is restored. Therefore, we can assess peroxisome function as a proxy for splicing efficiency. Although our alleles were not generated to study splicing, the range of splice-site mutants recovered and the simple peroxisome assays available make this system a facile platform to study splicing. It will be interesting to learn if additional *pex14* suppressors further illuminate the splicing machinery in plants.

Materials and methods

Plant material

Plants were from the Columbia-0 (Col-0) accession of Arabidopsis (*A. thaliana*), which was used as wild type. The *pex14-6 prp8a-14* double mutant identified in the suppression screen was backcrossed to *pex14-6* and then crossed to Col-0 to isolate the single *prp8a-14* mutant before phenotypic analysis. *pex14-4* (Monroe-Augustus et al., 2011), *pex14-6* (Burkhart et al., 2013), *pex14-7* (Fleming, 2016), and *pex14-12* (Fleming, 2016) were previously described. Homozygous double mutants were selected from progeny of *pex14-4*, *pex14-7*, or *pex14-12* crossed with backcrossed *pex14-6 prp8a-14* using polymerasae chain reaction (PCR)-based genotyping with the primers listed in Supplemental Table S2.

Growth conditions and physiological assays

Seeds were surface sterilized in 3% (v/v) NaOCl and 0.1% (v/v) Triton X-100, washed, suspended in 0.1% (w/v) agar, and stratified for 1–2 days in the dark at 4°C prior to plating. All growth assays were performed at 22°C. For dark-grown physiological assays, seeds were pre-germinated for 1 day in continuous white light prior to plating. For light and dark-grown assays, seeds were plated on plant nutrient media (Haughn and Somerville, 1986) solidified with 1% (w/v) agar and supplemented with 0.5% (w/v) sucrose and/or IBA as indicated. For dark-grown hypocotyl assays, plates were placed under continuous long-pass yellow-filtered light to slow IBA decomposition (Stasinopoulos and Hangarter, 1990) for 1 day and then wrapped in foil and positioned vertically for 4 days in the dark. For light-grown root assays, plates were positioned vertically under continuous long-pass yellow-filtered light for 8 days. Plates were imaged using a flatbed scanner, and hypocotyls (dark-grown seedlings) or roots (light-grown seedlings) were measured with ImageJ using the segment line and measure tools. Measurement data were graphed using the ggplot2 plug-in for RStudio software.

For monitoring phenotypes of mature plants, seeds were plated on 0.6% (w/v) agar-solidified plant nutrient media with 0.5% (w/v) sucrose and grown in continuous white light for 9 days and then transferred to soil and grown in continuous white light.

Mutant isolation and recombination mapping

pex14-6 seeds were mutagenized using 0.20% (v/v) EMS (Normanly et al., 1997) and 8 pools of M_2 seeds were surface-sterilized and screened for restored IBA sensitivity after 7 days on 8-μM IBA plant nutrient media plates with 0.5% (w/v) sucrose. Individuals with short roots were selected as putative *pex14-6* suppressors and moved to soil for immunoblot testing and propagation. Progeny from selected mutants was retested for IBA sensitivity and backcrossed to the parental *pex14-6* line. Backcrossed suppressors were identified using IBA responsiveness.

Whole-genome sequencing

Genomic DNA (gDNA) was isolated (Thole et al., 2014) from the pooled progeny of six plants from the backcross of a suppressor to *pex14-6* that displayed 100% IBA-sensitive roots. gDNA was sequenced by the Washington University Genome Technology Access Center using an Illumina HiSeq 2000. Sequencing data were aligned to Arabidopsis Col-0 with TAIR build 10 using Novoalign (Novocraft; http://novocraft.com). Mutations were identified with SAMtools (Li et al., 2009) and then annotated with snpEFF (Cingolani et al., 2012). Identified mutations were filtered for homozygous G-to-A or C-to-T point mutations that cause either nonsynonymous amino acid changes or splice-site changes (Farmer et al., 2013).

Immunoblot analysis

Protein extracts from seedlings grown on 0.6% (w/v) agar-solidified plant nutrient media with 0.5% (w/v) sucrose in continuous white light for 8 days were processed by grinding frozen tissue in a 1.7-mL microcentrifuge tube with a pestle. Ground tissue was suspended in 2× volume of sample buffer [106-mM Tris, pH 8.5, 2% (w/v) lithium dodecyl sulfate, 0.51-mM EDTA, pH 8.0, 10% (w/v) glycerol, 0.22-mM Coomassie blue G250, 0.166-mM phenol red (Invitrogen, Waltham, MA, USA)] supplemented with 50-mM DTT. Samples were incubated at 100°C for 5 min and centrifuged at 18,500 rcf for 5 min. Equal volumes of supernatants were loaded on Bolt 10% (w/v) Bis–Tris gels (Invitrogen) beside broad range prestained markers (New England Biolabs, Ipswich, MA, USA; P7712 or P7719). Samples were electrophoresed in MOPS running buffer (Invitrogen) and then transferred to Hybond-ECL nitrocellulose membrane (Amersham Pharmacia Biotech, Piscataway, NJ, USA; VWR 10120-006) using GenScript eBlot L1 western blotting transfer system according to recommendations of the manufacturer. Membranes were air-dried for 1 h then blocked in 8% (w/v) nonfat dry milk in Tris-buffered saline (TBS; 20-mM Tris, pH 7.5, 150-mM NaCl) for 1 h at room temperature before overnight incubation in primary antibody diluted in 8% nonfat dry milk in TBST (TBS with 0.1% (v/v) Tween-20) at 4°C. Membranes were rinsed 3 times with TBST and then incubated in horseradish peroxidase (HRP)-linked secondary antibody diluted in 8% nonfat dry milk in TBST for 2 h at room temperature. Membranes were rinsed in TBS, incubated in WesternSure PREMIUM chemiluminescent substrate (LI-COR 92695000), and imaged using an Odyssey Fc imaging system (LI-COR). Different primary antibodies were serially incubated and imaged on the same membrane without stripping. The primary antibodies used were rabbit anti-PEX14 (1:10,000 dilution; Agrisera AS08 372), rabbit anti-PMDH2 (1:5,000 dilution; Pracharoenwattana et al., 2007), and mouse anti-HSC70 (1:50,000 dilution, StressGen Bioreagents SPA-817). Secondary antibodies used were HRP-conjugated goat anti-rabbit (1:5,000 dilution, GenScript A00098) or anti-mouse (1:5,000 dilution, GenScript A00160) antibodies.

RNA isolation and analysis

Seedlings were grown for 8 days in continuous white light on sterilized Whatman 3 MM blotting paper atop 0.6% (w/v) agar-solidified plant nutrient media with 0.5% (w/v) sucrose. Seedlings frozen with liquid nitrogen were ground with a pestle, and RNA was extracted using RNeasy plant mini kits (Qiagen, Hilden, Germany; 74904).

For reverse transcription–PCR analysis, gDNA was removed from RNA (5–8 μg) using Invitrogen DNA-free DNA removal kit according to the recommendations of the manufacturer. DNAse-treated RNA was used as a template for cDNA synthesis using the 3′-gene-specific primers listed in Supplemental Table S1. To make cDNA, 1 μL of primer (2 μM) and 4 μL of dNTPs (2.5 mM) was added to the isolated RNA (10 μL) and incubated at 65°C for 5 min then transferred to ice for 1 min, after which 4 μL of 5× First strand buffer, 1 μL 0.1 DTT, 1 μL RNase Out, and 1 μL of Superscript III Reverse Transcriptase (Invitrogen; 18080-044) were added. Reactions were incubated at 50°C or 55°C for 1 h and then 70°C for 15–30 min.

To analyze individual splicing products, cDNAs were PCR-amplified using the primers listed in Supplemental Table S1, separated by electrophoresis in TAE gels containing 1% (w/v) agarose and 50 mM guanosine, and imaged with a Bio-Rad Gel Doc XR+. Individual amplicons were excised, and DNA was purified with QIAquick gel extraction kit (Qiagen; catalog: 28706) prior to Sanger sequencing at Genewiz.

RNA-seq library construction and sequencing analysis

RNA purified from 8-day-old light grown Col-0 and *prp8a-14* seedlings (three biological replicates) was sequenced at the Genome Technology Access Center of Washington University in St. Louis. Libraries were prepared from 5 to 10 μg of total RNA with an RIN (RNA integrity number) greater than 8.0 as determined using an Agilent Bioanalyzer or 4200 Tapestation. mRNA was enriched by poly-A selection using Oligo-dT beads (mRNA Direct kit, Life Technologies) and fragmented in reverse transcriptase buffer by heating to 94°C for 8 min. Fragmented mRNA was reverse transcribed to yield cDNA using SuperScript III RT enzyme (Life Technologies, Carlsbad, CA, USA) primed with random hexamers according to the manufacturer's instructions. A second strand reaction was performed to yield ds-cDNA. The cDNA was blunt ended, had an A base added to the 3′-ends, and then had Illumina sequencing adapters ligated to the ends. Ligated fragments were amplified for 12–15 cycles using primers incorporating unique dual index tags. Fragments were sequenced on an Illumina NovaSeq-6000 using paired-end reads extending 150 bases with a sequencing depth of 30 million reads per sample.

Adapters were trimmed using the bbduk program within BBTools (https://sourceforge.net/projects/bbmap/). Reads were aligned to the TAIR10 genome using HISAT2 (Kim et al., 2019) and counts were obtained using htseq-count (Anders et al., 2015). Differential expression was performed using PoissonSeq (Li et al., 2012) with a *q*-value cutoff of 0.05. Read counts were normalized to FPKM (fragments per kb per million mapped reads) before calculating fold changes.

Alternative splicing analysis

Alternative splicing sites were mapped and differential splicing events between Col-0 and the *prp8a-14* mutant were determined using rMATS (Shen et al., 2014). Skipped Exon (SE), Alternative 5′-splice site (A5SS), Alternative 3′-splice site (A3SS), Mutually Exclusive Exon (MXE), and Retained Intron (RI) events were determined based on the HISAT2 read alignment to the TAIR10 genome. After event detection, MXE events were removed from downstream analysis due to the low number identified (99). For the remaining four alternative SE, A5SS, A3SS, and RI, differentially spliced sites in the *prp8a-14* mutant were determined using rMATS with a $q < 0.05$

and a difference in splicing junction utilized of >0.05 (>5 percentage point difference in splicing junction utilized between Col-0 and *prp8a-14*). Sequence logos of utilized splice sites (4 nt on either side of exon/intron boundaries) were generated with WebLogo3 (Crooks et al., 2004) (http://weblogo.threeplusone.com/). Example RNA-seq reads spanning impacted 5′- or 3′-splice site were displayed using Integrative Genomics Viewer (IGV; Robinson et al., 2011).

GO enrichment analysis

GO enrichment analysis was performed using PANTHER (Thomas et al., 2003) against the gene models detected in the RNA-Seq dataset (26,895 genes) as the reference list. GO enrichment networks were constructed using ClueGo (Bindea et al., 2009).

Statistical analysis

Statistical analysis for physiological assays was performed with a one-way ANOVA (analysis of variance) with Tukey's post-hoc test using $P < 0.01$ (SPSS Statistics software, version 24.0.0.0). Hypergeometric tests for enrichment were performed using the *phyper* function in R. Two-tailed *z*-tests and two-sample Chi-squared tests were performed in JMP (https://www.jmp.com/).

Accession numbers

Sequence data from this article can be found in the GenBank/EMBL data libraries under accession numbers *At5g62810* (*PEX14*), *At1g80070* (*PRP8A*), and *At1g20960* (*BRR2A*). The raw and processed RNA-Seq data were submitted to the National Center for Biotechnology Information Gene Expression Omnibus database (Accession number GSE182779).

Supplemental data

The following materials are available in the online version of this article.

Supplemental Table S1. Primers for cDNA synthesis, amplification, and sequencing.

Supplemental Table S2. Genotyping primers and enzymes.

Supplemental Figure S1. *pex14* cDNA sequences in *pex14* mis-splicing mutants.

Supplemental Figure S2. Network analysis of significantly enriched GO terms of transcripts significantly downregulated (A) or upregulated (B) in *prp8a-14* seedlings.

Supplemental Figure S3. 5′- and 3′-splice sites utilized in differentially spliced wild-type and *prp8a-14* transcripts.

Supplemental Figure S4. Comparison of differentially expressed genes in *prp8a-14* and *brr2a-2*.

Supplemental Data Set 1. Differential expression analysis of *prp8a-14* versus wild type.

Supplemental Data Set 2. Differential splicing analysis of *prp8a-14* versus wild type.

Supplemental Data Set 3. Gene expression comparison of *prp8a-14* and *brr2a-2* mutants.

Acknowledgments

We thank Steven Smith (University of Tasmania) for the anti-PMDH2 antibody and Gabrielle Buck, Makaela Jackson, DurreShahwar Muhammad, Christopher Phillips, Nathan Tharp, Kathryn Smith, Ana Swearingen, Melissa Traver, and Zachary Wright for feedback on the manuscript. We thank the Genome Technology Access Center at the McDonnell Genome Institute at Washington University School of Medicine for help with whole-genome DNA sequencing and RNA sequencing.

Funding

This research was supported by the National Institutes of Health (NIH) grant R35GM130338 and the Robert A. Welch Foundation (C-1309) to B.B. R.J.L. was supported in part by the NIH (F31GM125367). N.M.C. was supported by a United States Department of Agriculture-National Institute of Food and Agriculture (USDA-NIFA) Postdoctoral Research Fellowship (2019-67012-29712). The Genome Technology Access Center is partially supported by a NIH National Cancer Institute Cancer Center Support Grant (P30CA91842) and by the NIH National Center for Research Resources ICTS/CTSA (UL1TR002345).

Conflict of interest statement. None declared.

References

Aebi M, Hornig H, Weissmann C (1987) 5′ cleavage site in eukaryotic pre-mRNA splicing is determined by the overall 5′ splice region, not by the conserved 5′ GU. Cell **50**: 237–246

Anders S, Pyl PT, Huber W (2015) HTSeq—a Python framework to work with high-throughput sequencing data. Bioinformatics **31**: 166–169

Azevedo JE, Schliebs W (2006) Pex14p, more than just a docking protein. Biochim Biophys Acta **1763**: 1574–1584

Ben-Yehuda S, Russell CS, Dix I, Beggs JD, Kupiec M (2000) Extensive genetic interactions between *PRP8* and *PRP17/CDC40*, two yeast genes involved in pre-mRNA splicing and cell cycle progression. Genetics **154**: 61–71

Bindea G, Mlecnik B, Hackl H, Charoentong P, Tosolini M, Kirilovsky A, Fridman WH, Pagès F, Trajanoski Z, Galon J (2009) ClueGO: a Cytoscape plug-in to decipher functionally grouped gene ontology and pathway annotation networks. Bioinformatics **25**: 1091–1093

Black DL, Steitz JA (1986) Pre-mRNA splicing in vitro requires intact U4/U6 small nuclear ribonucleoprotein. Cell **46**: 697–704

Black DL, Chabot B, Steitz JA (1985) U2 as well as U1 small nuclear ribonucleoproteins are involved in premessenger RNA splicing. Cell **42**: 737–750

Brody E, Abelson J (1985) The `spliceosome": yeast pre-messenger RNA associates with a 40S complex in a splicing-dependent reaction. Science **228**: 963–967

Burkhart SE, Lingard MJ, Bartel B (2013) Genetic dissection of peroxisome-associated matrix protein degradation in *Arabidopsis thaliana*. Genetics **193**: 125–141

Chabot B, Black DL, LeMaster DM, Steitz JA (1985) The 3′ splice site of pre-messenger RNA is recognized by a small nuclear ribonucleoprotein. Science **230**: 1344–1349

Chaudhary S, Khokhar W, Jabre I, Reddy ASN, Byrne LJ, Wilson CM, Syed NH (2019) Alternative splicing and protein diversity: plants versus animals. Front Plant Sci **10**: 708–722

Chen L, Bush SJ, Tovar-Corona JM, Castillo-Morales A, Urrutia AO (2014) Correcting for differential transcript coverage reveals a strong relationship between alternative splicing and organism complexity. Mol Biol Evol **31**: 1402–1413

Cheng SC, Abelson J (1987) Spliceosome assembly in yeast. Genes Dev **1**: 1014–1027

Cingolani P, Platts A, Wang LL, Coon M, Nguyen T, Wang L, Land SJ, Lu X, Ruden DM (2012) A program for annotating and predicting the effects of single nucleotide polymorphisms, SnpEff: SNPs in the genome of Drosophila melanogaster strain w1118; iso-2; iso-3. Fly (Austin) **6**: 80–92

Collins CA, Guthrie C (1999) Allele-specific genetic interactions between Prp8 and RNA active site residues suggest a function for Prp8 at the catalytic core of the spliceosome. Genes Dev **13**: 1970–1982

Crooks GE, Hon G, Chandonia JM, Brenner SE (2004) WebLogo: a sequence logo generator. Genome Res **14**: 1188–1190

Deng X, Lu T, Wang L, Gu L, Sun J, Kong X, Liu C, Cao X (2016) Recruitment of the nineteen complex to the activated spliceosome requires AtPRMT5. Proc Natl Acad Sci USA **113**: 5447–5452

Domdey H, Apostol B, Lin RJ, Newman A, Brody E, Abelson J (1984) Lariat structures are in vivo intermediates in yeast pre-mRNA splicing. Cell **39**: 611–621

Early P, Rogers J, Davis M, Calame K, Bond M, Wall R, Hood L (1980) Two mRNAs can be produced from a single immunoglobulin μ gene by alternative RNA processing pathways. Cell **20**: 313–319

Fabrizio P, Dannenberg J, Dube P, Kastner B, Stark H, Urlaub H, Lührmann R (2009) The evolutionarily conserved core design of the catalytic activation step of the yeast spliceosome. Mol Cell **36**: 593–608

Farmer LM, Rinaldi MA, Young PG, Danan CH, Burkhart SE, Bartel B (2013) Disrupting autophagy restores peroxisome function to an *Arabidopsis lon2* mutant and reveals a role for the LON2 protease in peroxisomal matrix protein degradation. Plant Cell **25**: 4085–4100

Fleming W (2016) Using forward genetics to identify novel *Arabidopsis thaliana* peroxisomal mutants. Thesis. Rice University, Houston, TX

Galej WP (2018) Structural studies of the spliceosome: past, present and future perspectives. Biochem Soc Trans **46**: 1407–1422

Galej WP, Oubridge C, Newman AJ, Nagai K (2013) Crystal structure of Prp8 reveals active site cavity of the spliceosome. Nature **493**: 638–643

Graham IA (2008) Seed storage oil mobilization. Annu Rev Plant Biol **59**: 115–142

Greene EA, Codomo CA, Taylor NE, Henikoff JG, Till BJ, Reynolds SH, Enns LC, Burtner C, Johnson JE, Odden AR, et al. (2003) Spectrum of chemically induced mutations from a large-scale reverse-genetic screen in *Arabidopsis*. Genetics **164**: 731–740

Haughn GW, Somerville C (1986) Sulfonylurea-resistant mutants of *Arabidopsis thaliana*. Mol Gen Genet **204**: 430–434

Hayashi M, Toriyama K, Kondo M, Nishimura M (1998) 2,4-Dichlorophenoxybutyric acid-resistant mutants of *Arabidopsis* have defects in glyoxysomal fatty acid beta-oxidation. Plant Cell **10**: 183–195

Hoskins AA, Friedman LJ, Gallagher SS, Crawford DJ, Anderson EG, Wombacher R, Ramirez N, Cornish VW, Gelles J, Moore MJ (2011) Ordered and dynamic assembly of single spliceosomes. Science **331**: 1289–1295

Kanno T, Lin WD, Fu JL, Matzke AJM, Matzke M (2017) A genetic screen implicates a CWC16/Yju2/CCDC130 protein and SMU1 in alternative splicing in *Arabidopsis thaliana*. RNA **23**: 1068–1079

Kao YT, Gonzalez KL, Bartel B (2018) Peroxisome function, biogenesis, and dynamics in plants. Plant Physiol **176**: 162–177

Kim D, Paggi JM, Park C, Bennett C, Salzberg SL (2019) Graph-based genome alignment and genotyping with HISAT2 and HISAT-genotype. Nat Biotechnol **37**: 907–915

Konarska MM, Grabowski PJ, Padgett RA, Sharp PA (1985) Characterization of the branch site in lariat RNAs produced by splicing of mRNA precursors. Nature **313**: 552–557

Konarska MM, Sharp PA (1987) Interactions between small nuclear ribonucleoprotein particles in formation of spliceosomes. Cell **49**: 763–774

Krainer AR, Maniatis T (1985) Multiple factors including the small nuclear ribonucleoproteins U1 and U2 are necessary for Pre-mRNA splicing in vitro. Cell **42**: 725–736

Kulichová K, Kumar V, Steinbachová L, Klodová B, Timofejeva L, Juříček M, Honys D, Hafidh SS (2020) PRP8A and PRP8B spliceosome subunits act coordinately to control pollen tube attraction in *Arabidopsis thaliana*. Development **147**: dev186742

Lerner MR, Boyle JA, Mount SM, Wolin SL, Steitz JA (1980) Are snRNPs involved in splicing? Nature **283**: 220–224

Lerner MR, Steitz JA (1979) Antibodies to small nuclear RNAs complexed with proteins are produced by patients with systemic lupus erythematosus. Proc Natl Acad Sci **76**: 5495–5499

Lesser CF, Guthrie C (1993) Mutational analysis of pre-mRNA splicing in *Saccharomyces cerevisiae* using a sensitive new reporter gene, *CUP1*. Genetics **133**: 851–863

Li H, Handsaker B, Wysoker A, Fennell T, Ruan J, Homer N, Marth G, Abecasis G, Durbin R (2009) The sequence alignment/Map format and SAMtools. Bioinformatics **25**: 2078–2079

Li J, Witten DM, Johnstone IM, Tibshirani R (2012) Normalization, testing, and false discovery rate estimation for RNA-sequencing data. Biostatistics **13**: 523–538

Linke WA (2008) Sense and stretchability: the role of titin and titin-associated proteins in myocardial stress-sensing and mechanical dysfunction. Cardiovasc Res **77**: 637–648

Liu L, Query CC, Konarska MM (2007) Opposing classes of *prp8* alleles modulate the transition between the catalytic steps of pre-mRNA splicing. Nat Struct Mol Biol **14**: 519–526

Mahrez W, Shin J, Muñoz-Viana R, Figueiredo DD, Trejo-Arellano MS, Exner V, Siretskiy A, Gruissem W, Köhler C, Hennig L (2016) BRR2a affects flowering time via *FLC* splicing. PLoS Genet **12**: e1005924

Marquardt S, Raitskin O, Wu Z, Liu F, Sun Q, Dean C (2014) Functional consequences of splicing of the antisense transcript *COOLAIR* on *FLC* transcription. Mol Cell **54**: 156–165

Marquez Y, Brown JWS, Simpson C, Barta A, Kalyna M (2012) Transcriptome survey reveals increased complexity of the alternative splicing landscape in *Arabidopsis*. Genome Res **22**: 1184–1195

Monroe-Augustus M, Ramón NM, Ratzel SE, Lingard MJ, Christensen SE, Murali C, Bartel B (2011) Matrix proteins are inefficiently imported into *Arabidopsis* peroxisomes lacking the receptor-docking peroxin PEX14. Plant Mol Biol **77**: 1–15

Mount SM (1982) A catalogue of splice junction sequences. Nucleic Acids Res **10**: 459–472

Mount SM, Pettersson I, Hinterberger M, Karmas A, Steitz JA (1983) The U1 small nuclear RNA-protein complex selectively binds a 5′ splice site in vitro. Cell **33**: 509–518

Nguyen THD, Li J, Galej WP, Oshikane H, Newman AJ, Nagai K (2013) Structural basis of Brr2-Prp8 interactions and implications for U5 snRNP biogenesis and the spliceosome active site. Structure **21**: 910–919

Nilsen TW, Graveley BR (2010) Expansion of the eukaryotic proteome by alternative splicing. Nature **463**: 457–463

Normanly J, Grisafi P, Fink GR, Bartel B (1997) *Arabidopsis* mutants resistant to the auxin effects of indole-3-acetonitrile are defective in the nitrilase encoded by the *NIT1* gene. Plant Cell **9**: 1781–1790

Parker R, Siliciano PG, Guthrie C (1987) Recognition of the TACTAAC box during mRNA splicing in yeast involves base pairing to the U2-like snRNA. Cell **49**: 229–239

Pracharoenwattana I, Cornah JE, Smith SM (2007) *Arabidopsis* peroxisomal malate dehydrogenase functions in β-oxidation but not in the glyoxylate cycle. Plant J **50**: 381–390

Query CC, Konarska MM (2004) Suppression of multiple substrate mutations by spliceosomal *prp8* alleles suggests functional correlations with ribosomal ambiguity mutants. Mol Cell **14**: 343–354

Robinson JT, Thorvaldsdóttir H, Winckler W, Guttman M, Lander ES, Getz G, Mesirov JP (2011) Integrative genomics viewer. Nat Biotechnol **29**: 24–26

Rogers J, Wall R (1980) A mechanism for RNA splicing. Proc Natl Acad Sci **77**: 1877–1879

Sasaki T, Kanno T, Liang SC, Chen PY, Liao WW, Lin WD, Matzke AJM, Matzke M (2015) An Rtf2 domain-containing protein influences pre-mRNA splicing and is essential for embryonic development in *Arabidopsis thaliana*. Genetics **200**: 523–535

Schaub A, Glasmacher E (2017) Splicing in immune cells—mechanistic insights and emerging topics. Int Immunol **29**: 173–181

Schwartz B, Yeung E, Meinke D (1994) Disruption of morphogenesis and transformation of the suspensor in abnormal suspensor mutants of *Arabidopsis*. Dev Camb Engl **120**: 3235–3245

Seo PJ, Kim MJ, Ryu JY, Jeong EY, Park CM (2011) Two splice variants of the IDD14 transcription factor competitively form nonfunctional heterodimers which may regulate starch metabolism. Nat Commun **2**: 303

Seraphin B, Kretzner L, Rosbash M (1988) A U1 snRNA:pre-mRNA base pairing interaction is required early in yeast spliceosome assembly but does not uniquely define the 5′ cleavage site. EMBO J **7**: 2533–2538

Seraphin B, Rosbash M (1989) Identification of functional U1 snRNA-pre-mRNA complexes committed to spliceosome assembly and splicing. Cell **59**: 349–358

Seraphin B, Abovich N, Rosbash M (1991) Genetic depletion indicates a late role for U5 snRNP during in vitro spliceosome assembly. Nucleic Acids Res **19**: 3857–3860

Shen S, Park JW, Lu ZX, Lin L, Henry MD, Wu YN, Zhou Q, Xing Y (2014) rMAT S: robust and flexible detection of differential alternative splicing from replicate RNA-Seq data. Proc Natl Acad Sci USA **111**: E5593–601

Siatecka M, Reyes JL, Konarska MM (1999) Functional interactions of Prp8 with both splice sites at the spliceosomal catalytic center. Genes Dev **13**: 1983–1993

Siliciano PG, Guthrie C (1988) 5′ splice site selection in yeast: genetic alterations in base-pairing with U1 reveal additional requirements. Genes Dev **2**: 1258–1267

Stasinopoulos TC, Hangarter RP (1990) Preventing photochemistry in culture media by long-pass light filters alters growth of cultured tissues. Plant Physiol **93**: 1365–1369

Strader LC, Wheeler DL, Christensen SE, Berens JC, Cohen JD, Rampey RA, Bartel B (2011) Multiple facets of *Arabidopsis seedling development require indole-3-butyric acid–derived auxin*. Plant Cell **23**: 984–999

Thole JM, Beisner ER, Liu J, Venkova SV, Strader LC (2014) Abscisic acid regulates root elongation through the activities of auxin and ethylene in *Arabidopsis thaliana*. Genes Genomes Genet **4**: 1259–1274

Thomas PD, Campbell MJ, Kejariwal A, Mi H, Karlak B, Daverman R, Diemer K, Muruganujan A, Narechania A (2003) PANTHER: a library of protein families and subfamilies indexed by function. Genome Res **13**: 2129–2141

Turner IA, Norman CM, Churcher MJ, Newman AJ (2006) Dissection of Prp8 protein defines multiple interactions with crucial RNA sequences in the catalytic core of the spliceosome. RNA **12**: 375–386

Wahl MC, Will CL, Lührmann R (2009) The spliceosome: design principles of a dynamic RNP machine. Cell **136**: 701–718

Wan R, Yan C, Bai R, Huang G, Shi Y (2016) Structure of a yeast catalytic step I spliceosome at 3.4 A resolution. Science **353**: 895–904

Wang BB, Brendel V (2006) Genomewide comparative analysis of alternative splicing in plants. Proc Natl Acad Sci USA **103**: 7175–7180

Winkelmann G, Bach M, Lührmann R (1989) Evidence from complementation assays in vitro that U5 snRNP is required for both steps of mRNA splicing. EMBO J **8**: 3105–3112

Yan C, Wan R, Bai R, Huang G, Shi Y (2017) Structure of a yeast step II catalytically activated spliceosome. Science **355**: 149–155

Zhuang Y, Weiner AM (1986) A compensatory base change in U1 snRNA suppresses a 5′ splice site mutation. Cell **46**: 827–835

Zolman BK, Yoder A, Bartel B (2000) Genetic analysis of indole-3-butyric acid responses in *Arabidopsis thaliana* reveals four mutant classes. Genetics **156**: 1323–1337